European Polymer Journal 45 (2009) 1924–1935

Contents lists available at ScienceDirect

European Polymer Journal

journal homepage: www.elsevier.com/locate/europolj

Macromolecular Nanotechnology

Hydrogen bond mediated supramolecular micellization of diblock copolymer mixture in common solvents

Shiao-Wei Kuo [a,*], Pao-Hsaing Tung [b], Feng-Chih Chang [b]

[a] Department of Materials Science and Optoelectronic Engineering, Center for Nanoscience and Nanotechnology, National Sun Yat-Sen University, Kaohsiung 804, Taiwan
[b] Institute of Applied Chemistry, National Chiao Tung University, Hsinchu 30050, Taiwan

ARTICLE INFO

Article history:
Received 21 October 2008
Received in revised form 11 March 2009
Accepted 29 March 2009
Available online 5 April 2009

Keywords:
Diblock copolymer
Self-assembly
Hydrogen bonding
Micelle

ABSTRACT

We report a new approach toward preparing self-assembled hydrogen-bonded complexes having vesicle and patched spherical structures from two species of block copolymers in nonselective solvents. Two diblock copolymers, poly(styrene-*b*-vinyl phenol) (PS-*b*-PVPh) and poly(methyl methacrylate-*b*-4-vinylpyridine) (PMMA-*b*-P4VP), were synthesized through anionic polymerization. The assembly of vesicles from the intermolecular complex formed after mixing PS-*b*-PVPH with PMMA-*b*-P4VP in THF was driven by strong hydrogen bonding between the complementary binding sites on the PVPH and P4VP blocks. In contrast, well-defined patched spherical micelles formed after blending PS-*b*-PVPh with PMMA-*b*-P4VP in DMF: the weaker hydrogen bonds formed between the PVPh and P4VP blocks in DMF, relative to those in THF, resulted in the formation of spherical micelles having compartmentalized coronas consisting of PS and PMMA blocks.

1. Introduction

Diblock copolymers continue to be the focus of an immense amount of research because of their abilities to self-assemble into well-defined nanostructures and sizes. As a result, many types of diblock copolymers have been synthesized and their characteristic nano- and microphase separation structures studies in bulk and solution states [1–13]. Polymeric micelles that contain an insoluble block core and are surrounded by a corona of a solvated block can exhibit fascinating nanostructures, including spherical, cylindrical, lamellar, and vesicular micelles [14,15]. In particular, because of their small sizes and high stabilities, polymeric micelles have received significant attentions for use in drug delivery, as templates for the preparation of inorganic nanoparticles (including metals, metal oxides, and semiconductors), and as traps for environmental pollutants or metabolites [16–22].

More-complex macromolecules, such as ABC triblock copolymers, have been attracted much interest in recent years. Although their self-assembly in solution remains somewhat unexplored, several triblock copolymer morphologies have been characterized in both aqueous and organic media. Because the synthesis of ABC triblock copolymers is relatively complex, mixing A–B with B–C or C–D diblock copolymers is a somewhat simpler approach toward exploring these systems' morphological behavior. The simplest case involves mixing an A-*b*-B diblock copolymer with a C homopolymer or a C-*b*-D diblock copolymer in solution state. If specific interactions exist between the C block and one of the blocks in the A-*b*-B, inter-polymer complex micelles can be formed from the complementary polymers [23–27]. The assembly of such non-covalently bonded micelles can be mediated by inter-polymer hydrogen bonding [28–37], electrostatic interactions [38–41], and metal–ligand coordinative bond [42,43]. In general, the shapes of these supramolecular structures can be classified into three types: (i) core–shell spherical micelles having an insoluble complex core and a

* Tel.: +886 7 5252000x4079; fax: +886 7 5254099.
E-mail address: kuosw@faculty.nsysu.edu.tw (S.-W. Kuo)

0014-3057/$ - see front matter © 2009 Elsevier Ltd. All rights reserved.
doi:10.1016/j.eurpolymj.2009.03.020

soluble block as the corona [33,37], (ii) onion-type (core–shell–corona (CSC) micelles) having an insoluble core A, a shell composed of a B–C inter-polymer complex, and a corona formed by a soluble block D [31,32], and (iii) vesicles from A-*b*-B and C-*b*-D copolymers having two insoluble segments (A and D) and mutually interacting B and C blocks [28–30,44]. If the two blocks composing the core are sufficiently large and mutually immiscible, they will most likely segregate into different phases, forming two separate compartments in the core of the micelle. Nevertheless, depending upon the molecular structure of the segments, diverse morphologies can be expected for a multi-compartmentalized core [45,46]. Micelles displaying a compartmentalized corona have been observed also for systems possessing two immiscible coronal blocks [28–30].

Herein, we report a facile method for the preparation of stable micellar complexes in nonselective solvents mediated by the hydrogen-bonding interactions between poly(styrene-*b*-vinyl phenol) (PS-*b*-PVPh, denoted "A-*b*-B") and poly(4-vinylpyridine-*b*-methyl methacrylate) (P4VP-*b*-PMMA, denoted as "C-*b*-D"). Because the P4VP and PVPh blocks contain strong proton acceptor groups and strong proton donor groups, respectively, strong hydrogen bonding occurs between these donors and acceptors in THF and DMF solutions, as has been demonstrated by FTIR spectroscopy. In addition, it is well known that the solvent medium plays an important role in affecting or controlling the types of complex formed [47,48]. For instance, the PVPh/P4VP mixtures yield the complex precipitates in THF, whereas no precipitation occurs from DMF. Because solvent molecules can also participate in hydrogen-bonding interactions, they compete with P4VP for binding with the hydroxyl groups in PVPh. The affinity of the hydrogen bond acceptor can be estimated by comparing the difference between the IR absorption frequencies ($\Delta\nu$) of hydrogen-bonded and free hydroxyl units of phenol (a model compound for PVPh) [44]. Using this approach, THF is found to be a relatively weaker hydrogen bond acceptor ($\Delta\nu = 235\ cm^{-1}$) than is DMF ($\Delta\nu = 340\ cm^{-1}$). Indeed, DMF is such a strong hydrogen bond disrupting solvent that it does not allow the formation of the inter-polymer complex [47,48]. In previous studies, we concentrated on determining the effect of hydrogen bonding on polymer miscibility and inter-polymer complexation [49–54]. Base on our long-term interest in polymer miscibility and complexation through hydrogen bonding, we are extending our studies to investigate new approaches toward hydrogen bond-related polymer micellization. Most importantly, the polymer chain behavior of PVPh/P4VP systems in solvents that are less polar solvent than DMF, such as THF, dioxane, acetone, and methanol tends to result in complex aggregates, whereas they form separated chains in DMF [55]. The PVPH blocks interact with P4VP chains in these inter-polymer hydrogen-bonded complex micelles. Paris of block copolymers have been observed to self-assemble into the form of vesicles in THF solution [mediated by strong hydrogen bonds between PVPh and P4VP] and patched spherical micelles in DMF solution [PVPh/P4VP] cores surrounding by mixed PS and PMMA chains in the corona]. Scheme 1 provides a schematic illustration the formation of inter-polymer hydrogen-bonded complexes induced by hydrogen-bonding interactions between P4VP and PVPh blocks in two types of nonselective solvents.

2. Experimental

2.1. Diblock copolymers syntheses

Diblock copolymers of poly(styrene-*b*-4-*tert*-butoxyystyrene) (PS-*b*-P*t*BOS) were synthesized through sequential anionic polymerization of styrene followed by 4-*tert*-butoxystyrene using *sec*-butyl lithium as the initiator [56,57]. After the polymerizations were complete and then quenched with degassed methanol. The product was precipitated in methanol and dried in a vacuum oven. This precursor block copolymer was hydrolyzed to PS-*b*-PVPh by heating them in 1,4-dioxane for 24 h under reflux at 85 °C in the presence of concentrated HCl as the catalyst. The final product was neutralized and purified through the Soxhlet extraction with water for 72 h before being

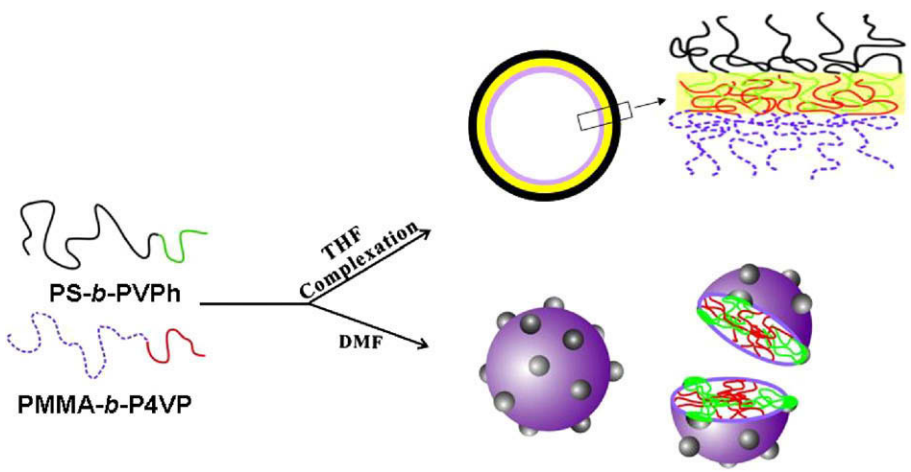

Scheme 1. Models of micelle formation mediated by hydrogen-bonding interactions between SVPh/MVP diblock copolymers mixtures.

dried under vacuum at 80 °C. A detailed description and characterization of the procedure has been reported previously [58,59]. The block copolymers are designed as PS_{90}-*b*-$PVPH_{10}$ (SVPh90-10) and PS_{20}-*b*-$PVPh_{80}$ (SVPh20-80), where the numbers in parentheses are the molecular molar fractions (mol%). Diblock copolymers of poly(methyl methacrylate-*b*-4-vinylpyridine) (PMMA-*b*-P4VP) were synthesized using the same polymerization procedure. Total molecular weights of these two kinds of block copolymers and their mole fractions are summarized in Table 1.

2.2. Preparation of PS-b-PVPh/PMMA-b-P4VP micelle solutions

For the solution assembly of PS-*b*-PVPh and PMMA-*b*-P4VP, these two diblock copolymers were dissolved individually in common solvents (THF and DMF), filtered through a membrane having a nominal pore size of 0.2 μm to remove dust, and then mixed at ambient temperature. Mixtures of desired solutions with PS-*b*-PVPh/PMMA-*b*-P4VP (M_{SH}/M_{MVP}) molar ratios ranging from 0.25 (1:4) to 2 (1:0.5) were stirred for more than 24 h at room temperature. The PVPh block is expected to interact with the P4VP units through hydrogen-bonding interaction. These diblock copolymers were mixed in THF and DMF solutions, both of which are good solvents for PS and PMMA blocks, leading to formation of micelles possessing a PVPh/P4VP core surrounded by a mixed corona of PS and PMMA blocks.

2.3. Characterizations

Infrared spectra were recorded at 25 °C at a resolution of 1 cm^{-1} on a Nicolet AVATAR 320 FTIR spectrometer using polymer films that had been cast onto KBr pellets from THF or DMF solution and then vacuum-dried. All FTIR spectra were obtained within the spectral range 4000–400 cm^{-1} from 32 scans collected at a resolution of 1 cm^{-1}; the samples were purged with nitrogen to maintain each film's dryness. The hydrodynamic diameters of the assemblies were measured by dynamic light scattering (DLS) using a Brookheaven 90 plus instrument (Brookheaven Instruments Corporation, USA) equipped with a He–Ne laser operated at a power of 35 mW at 632.8 nm. All DLS measurements were performed using with a wavelength of 632.8 nm at 25 °C and an angle of 90°. For transmission electron microscopy (TEM) studies, a drop of the resulting micelle solution was sprayed onto a copper TEM grid covered with a Formvar supporting film that had been pre-coated with a thin film of carbon. All samples were left to dry at room temperature for 1 day before observation. After 1 min, the excess solvent was blotted away using a strip of filter paper. All samples were stained with ruthenium tetraoxide (RuO_4) or iodine (I_2) and then viewed under a Hitachi, H-7500 transmission electron microscope (TEM) operated at an accelerating voltage of 100 kV. In TEM images, RuO_4 staining generally results in P4VP, PVPh, PS, and PMMA blocks appearing with dark, intermediate, light, and very light contrasts, respectively; the P4VP domain is stained selectively with I_2.

3. Results and discussion

We used IR spectroscopy, TEM, and dynamic light scattering to analyze the non-covalently connected polymeric micelles formed from mixtures of PS-*b*-PVPh and PMMA-*b*-P4VP diblock copolymers. In THF or DMF solvent, both are good solvents for PS and PMMA blocks, the micelles that formed possessed PVPh/P4VP cores surrounding by mixed coronas of PS and PMMA blocks. Although the hydrogen-bonding interactions between the PVPh and PMMA blocks is substantially weaker than those between PVPh and P4VP, these interactions cannot be disregarded, especially at higher PVPh contents.

3.1. Infrared analyses

FTIR spectroscopy has been applied to the analysis of numerous diblock copolymers and blends that interact intermolecularly through hydrogen bonding [49]. The strength of complexation through hydrogen bonding is strongly influenced by the solvent used. Fig. 1 displays room-temperature IR spectra of the hydroxyl group stretchings of the PS-*b*-PVPh/PMMA-*b*-P4VP mixtures cast from THF and DMF solutions. The spectrum of pure PVPh shows two unresolved bands in the hydroxyl-stretching region, corresponding to the free hydroxyl units at 3525 cm^{-1} and a broad band centered at 3400 cm^{-1} for the absorption of self-associated hydrogen-bonded hydroxyl groups. The peak frequency of the broad band shifts to lower wavenumber in the spectrum of the 1:1 PS-*b*-PVPh/PMMA-*b*-P4VP diblock copolymer blends, and becomes broader than pure PS-*b*-PVPh copolymer, reflecting that a new distribution of hydrogen bonds had resulted from competition between the hydroxyl–hydroxyl [within the pure PVPh], hydroxyl–pyridine [between PVPh and P4VP], and hydroxyl–carbonyl [between PVPh and PMMA] interactions. In the THF system, we observe a lower intensity of the signal for the free hydro-

Table 1
Molecular characteristic of PS-*b*-PVPh and PMMA-*b*-P4VP copolymers.

Diblock copolymers	M_n		M_w/M_n[a]	Mole fraction [b]			
	1st segment[a]	2nd segment[b]		ψ_S	ψ_H	ψ_M	ψ_P
PS_{90}-*b*-$PVPh_{10}$ (SH90-10)	37,500	4300	1.10	90	10		
PS_{20}-*b*-$PVPh_{80}$ (SH20-80)	3600	16,000	1.13	18	82		
$PMMA_{80}$-*b*-$P4VP_{20}$ (MVP80-20)	15,000	4300	1.18			78	22
$PMMA_{35}$-*b*-$P4VP_{65}$ (MVP35-65)	7450	14,000	1.21			35	65

[a] Obtained from GPC analysis.
[b] Calculated from ^1H NMR spectrum.

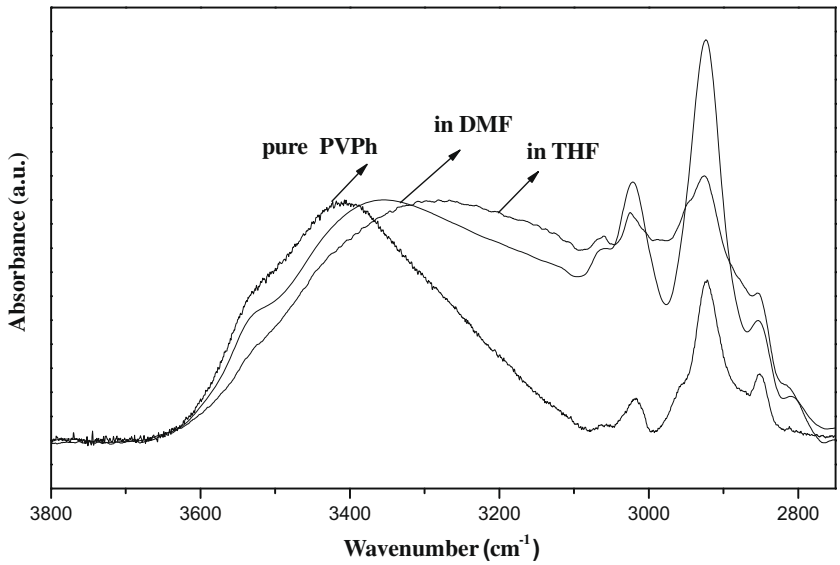

Fig. 1. FTIR spectra, recorded at room temperature, of the hydroxyl region of the diblock copolymer mixture (1/1 molar ratio) cast from THF and DMF solutions.

xyl groups and a lower wavenumber (3280 cm^{-1}) for the broad band than those in the DMF system (3360 cm^{-1}), suggesting that stronger hydrogen-bonding interactions occur in THF than in DMF [49].

Fig. 2 presents several regions of the IR spectra recorded at room temperature of various PS_{20}-*b*-$PVPh_{80}$/$PMMA_{35}$-*b*-$P4VP_{65}$ (SH20-80/MVP35-65) mixtures namely the (A) hydroxyl stretching (2700–3800 cm^{-1}), (B) carbonyl stretching (1670–1760 cm^{-1}), and (C) pyridine ring absorption (970–1030 cm^{-1}) regions, which are all influenced by hydrogen-bonding interactions. Clearly, the hydroxyl stretching intensities of the SH20-80/MVP35-65 mixtures shifted to lower wavenumber upon increasing the $PMMA_{35}$-*b*-$P4VP_{65}$ content, as indicated in Fig. 2(A). In addition, the hydroxyl stretching band broadened because it was composed of contributions from several different environments surrounding the hydroxyl groups, i.e., many different types of hydroxyl groups are present in the SVPh20-80/MVP35-65 mixtures. The signals for hydroxyl groups that formed inter-association hydrogen-bonds with pyridine rings appeared at relatively lower wavenumber than hydroxyl–carbonyl group (depending on the $PMMA_{35}$-*b*-$P4VP_{65}$ diblock copolymer content). At a lower PS-*b*-PVPh content, most hydroxyl groups are hydrogen bonded with pyridine groups revealing that the interaction between PVPh and P4VP becomes dominant and at a lower

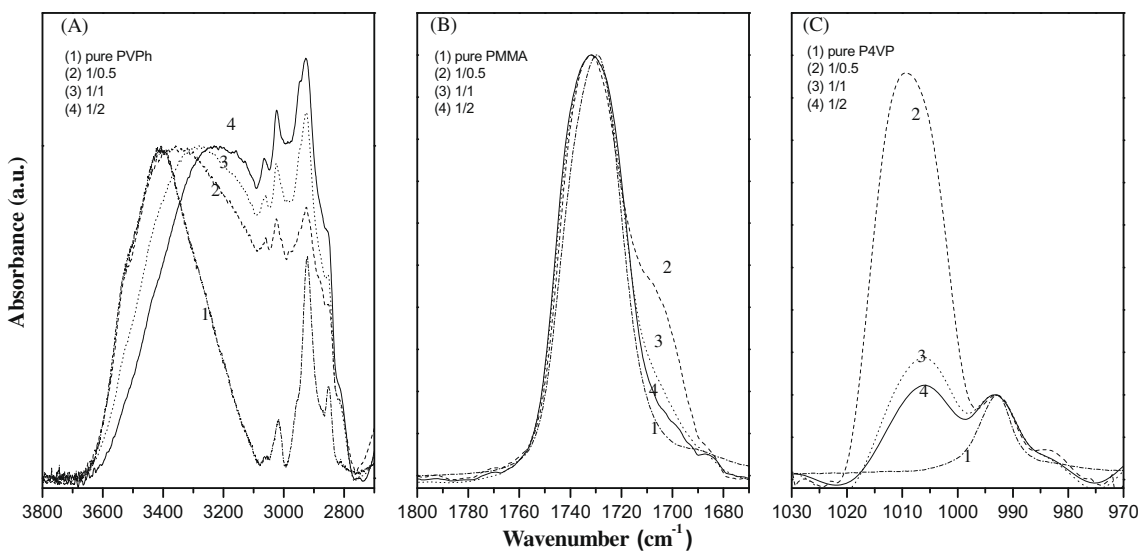

Fig. 2. FTIR spectra of SVPh20-80/MVP35-65 in THF at room temperature; (A) hydroxyl stretching band (2700–3800 cm^{-1}), (B) carbonyl stretching band (1670–1760 cm^{-1}), and (C) pyridine ring absorption (970–1030 cm^{-1}).

PS-*b*-PVPh content, and the interaction between PVPh and PMMA are observed at relative high wavenumber.

Fig. 2(B) shows the carbonyl stretching region (1670–1760 cm^{-1}) of the IR spectra of PMMA at various SVPh20-80/MVP35-65 molar ratios in THF. For the non-covalently complex micelles, Fig. 2(B) indicates that the location of this band was highly dependent on the SVPh20-80/MVP35-65 molar ratio. The peaks at 1730 and 1706 cm^{-1} are those of the free and hydrogen-bonded carbonyl groups, respectively. As the molar ratio PMMA-*b*-P4VP increased, we fraction of hydrogen-bonded carbonyl groups are decreased, indicating that the hydrogen-bonding interaction between PVPh and P4VP is stronger than interaction PVPh and PMMA.

In addition to the hydroxyl and carbonyl stretching regions, the characteristic signals of the pyridine rings are also sensitive to the extent of hydrogen bonding. Herein, we used the band at 993 cm^{-1} as a probe to characterize the hydrogen-bonding interactions between the hydroxyl groups of PVPh and the pyridine groups of P4VP; unfortunately, the band at 1590 cm^{-1} for P4VP was difficult to analyze because of its overlap with the band at 1600 cm^{-1} for PVPh. Fig. 2(C) presents scale-expanded infrared spectra in the range 970–1030 cm^{-1} measured at room temperature for various SVPh20-80/MVP35-65 copolymer mixtures. Pure P4VP has a characteristic band at 993 cm^{-1} corresponding to the absorption of an uncomplexed pyridine ring. We assign the new band at 1006 cm^{-1} to hydrogen-bonded pyridine units; its intensity increases upon the addition of PVPh blocks to P4VP blocks. All these carbonyl and pyridine ring frequencies in Fig. 2(B) and (C) split into two bands that can be fitted well to the Gaussian function and results from curve fitting are summarized in Table 2, the hydrogen bonding fraction of the carbonyl and pyridine ring increases with the increase of the PVPh content in these diblock copolymers blends. All IR spectra show the existence of hydrogen-bonding interaction between the pyridine group and the hydroxyl group at all molar ratios, however, the more hydrogen-bonding interaction fraction between PVPh and PMMA is only existed at relatively higher PVPh content. In summary, the hydrogen-bonding interaction in PS-*b*-PVPh/PMMA-*b*-P4VP diblock blend system is following this order: PVPh—P4VP [60] > PVPh—PVPh [49] > PVPh—PMMA [49], which is consistent with the Painter–Coleman association model (PCAM) as shown in Table 3.

It is clear that the PVPh hydroxyl is able to form hydrogen bonds with both P4VP and PMMA. According to the Painter–Coleman association model (PCAM) [49], we designate B, A, and C as PVPh, PCL, and P4VP, respectively, and K_2, K_B, K_A, and K_C as their corresponding association equilibrium constants. These four equilibrium constants can be expressed as follows in terms of volume fractions

$$\Phi_B = \Phi_{B1}\Gamma_2\left[1+\frac{K_A\Phi_{A1}}{r_A}+\frac{K_C\Phi_{C1}}{r_C}\right] \quad (1)$$

$$\Phi_A = \Phi_{A1}[1+K_A\Phi_{B1}\Gamma_1] \quad (2)$$

$$\Phi_C = \Phi_{C1}[1+K_C\Phi_{B1}\Gamma_1] \quad (3)$$

where

$$\Gamma_1 = \left(1-\frac{K_2}{K_B}\right)+\frac{K_2}{K_B}\left(\frac{1}{1-K_B\Phi_{B1}}\right) \quad (4)$$

$$\Gamma_2 = \left(1-\frac{K_2}{K_B}\right)+\frac{K_2}{K_B}\left(\frac{1}{(1-K_B\Phi_{B1})^2}\right) \quad (5)$$

Table 3
Summary of the self- and inter-association equilibrium constants, and their thermodynamic parameter of PS-*b*-PVPh/PMMA-*b*-P4VP at 25 °C.

Polymer	V	M_w	δ	Equilibrium constant		
				K_2	K_B	K_A
PVPh[a]	100.0	120.0	10.6	21.0	66.8	
P4VP[b]	84.9	105.1	10.8			1400[b]
PMMA[a]	84.9	100.2	9.1			37.4
PS[a]	93.9	104.0	9.5			

V, molar volume (ml/mol); M_w, molecular weight (g/mol); δ, solubility parameter $(cal/ml)^{1/2}$; DP, degree of polymerization; K_2, dimer self-association equilibrium constant; K_B, multimer self-association equilibrium constant; K_A, inter-association equilibrium constant.
[a] Ref. [49].
[b] Ref. [61].

Table 2
Curve fitting of hydrogen bonding results of PS-*b*-PVPh/PMMA-*b*-P4VP at 25 °C.

PS-*b*-PVPh/PMMA-*b*-P4VP	Free carbonyl			H-bond carbonyl			$f_b^{C=O}$[a]
	ν, cm^{-1}	$W_{1/2}$, cm^{-1}	A_f (%)	ν, cm^{-1}	$W_{1/2}$, cm^{-1}	$A_{b\%}$	
Pure PMMA	1730	25	100.0				
1/2	1732	26	88.7	1706	20	11.3	7.0
1/1	1732	26	87.6	1706	20	12.4	8.6
2/1	1732	26	76.4	1706	20	23.6	17.0
	Free pyridine ring			H-bonded pyridine ring			$f_b^{pyridine}$[b]
	ν, cm^{-1}	$W_{1/2}$, cm^{-1}	A_f (%)	ν, cm^{-1}	$W_{1/2}$, cm^{-1}	$A_{b\%}$	
Pure P4VP	993	11	100.0	–	–	–	–
1/2	993	10	42.0	1005	11	58.0	58.0
1/1	993	10	35.5	1005	11	64.5	64.5
2/1	993	10	13.7	1006	11	86.3	86.3

[a] $f_b^{C=O}$, fraction of hydrogen bonding carbonyl $= \frac{A_b/1.5}{A_b/1.5+A_f}$.
[b] $f_b^{pyridine}$, fraction of hydrogen bonding pyridine $= \frac{A_b}{A_b+A_f}$.

Φ_B, Φ_A, and Φ_C are the volume fractions of repeat units in the blend, Φ_{B1}, Φ_{A1}, and Φ_{C1} are the volume fractions of isolated units in the blend, and $r_A = V_A/V_B$ and $r_C = V_C/V_B$ are the ratios of segmental molar volumes.

The self-association constants of PVPh ($K_2 = 21.0$ and $K_B = 66.8$) and the inter-association constant between PVPh and P4VP ($K_C = 598$) have been determined [49]. The inter-association constant K_A value is determined directly from a least squares fitting procedure based on the fraction of hydrogen-bonded carbonyl experimentally obtained in the binary PVPh/PMMA blend ($K_A = 37.5$) [49]. Table 3 lists all the parameters required by the PCAM to estimate thermodynamic properties for these blends. If we know these equilibrium constants (K_2, K_B, K_C, and K_A) and segment molar volumes, the fraction of hydrogen-bonded carbonyl group and pyridine can be calculated from Eqs. (1)–(5) using $f_{HB} = 1 - \frac{\Phi_{C1}}{\Phi_C}$. Therefore, the predicted fraction of hydrogen bonding of carbonyl groups shown in Fig. 3 can be calculated numerically.

Fig. 3 plots the experimental data and the prediction curves by using the PCAM model of PMMA-*b*-P4VP/PS-*b*-PVPh vs. PS-*b*-PVPh weight fraction of these four blend systems from the FTIR of hydrogen-bonded carbonyl and pyridine region. It is worth to note that there is a large negative deviation of PMMA hydrogen-bonded carbonyl group, but gives a slight deviation of P4VP hydrogen-bonded pyridine group from PCAM prediction curve. Clearly, increase the composition of PVPh in block copolymers, the larger deviation from experiment and prediction data was found in hydrogen-bonded carbonyl group, but gives only a relatively smaller deviation in hydrogen-bonded pyridine group. The main reason from deviation is the inter-association equilibrium constant of PVPh/P4VP is significantly greater than PVPh/PMMA, thus the PMMA would exclude from PVPh/P4VP phase. The microphase separation of PMMA block would decrease the intermolecular hydrogen-bonding interaction between PVPh and PMMA; as a result, the experimental data of hydrogen-bonded carbonyl group is lower than predicted data.

3.2. Structures and properties of PS-*b*-PVPh/PMMA-*b*-P4VP micelles in THF solution

We used TEM to characterize the various morphologies of these non-covalently bond micelles. Here, we discuss the structure of the PS-*b*-PVPh/PMMA-*b*-P4VP system, which comprised two asymmetric block copolymers, with similar molecular weights and lengths of the PVPh and P4VP blocks, where the attractive interactions between the PVPh and P4VP blocks allowed complementary polymer pairs to assemble into micelles. Firstly, we describe TEM images of SVPh90-10/MVP80-20 hydrogen-bonded complexes formed in THF solution at various ratios. TEM images of the 1:2 and 1:1 SVPh90-10/MVP80-20 systems, stained with I_2, are presented in Fig 4(A) and (C), respectively. These images display structures in the shape of highly polydisperse hollow spheres, but further information was difficult to achieve because of poor contrast. Therefore, we performed additional staining with RuO_4; Fig. 4(B), (D), and (E) display the comparative results. The contrast in the images of these RuO_4-stained complexed micelles was better than in the images obtained with I_2 staining; indeed, it became clear that these complex micelles all possessed vesicular structures.

Because PVPH contains the strong proton donor groups and P4VP behaves as a proton acceptor through the nitrogen atoms on its pyridine rings, the P4VP blocks probably formed intermolecular hydrogen bonds with the PVPh blocks. The inter-polymer hydrogen-bonded complexation between PS-*b*-PVPh and PMMA-*b*-P4VP would lead to the formation the cores of PVPh/P4VP chain aggregates with strong hydrogen-bonding interactions, low chain mobility,

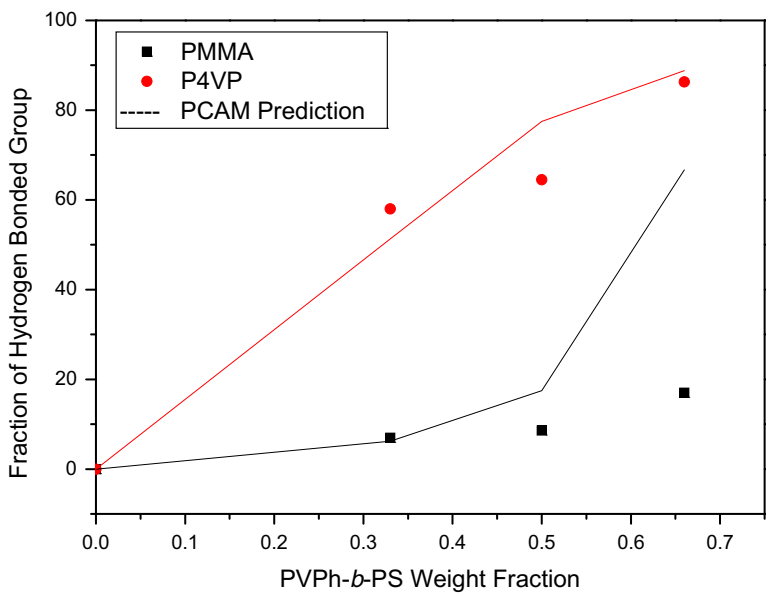

Fig. 3. Experimental data of hydrogen-bonded carbonyl pyridine group with PCAM prediction.

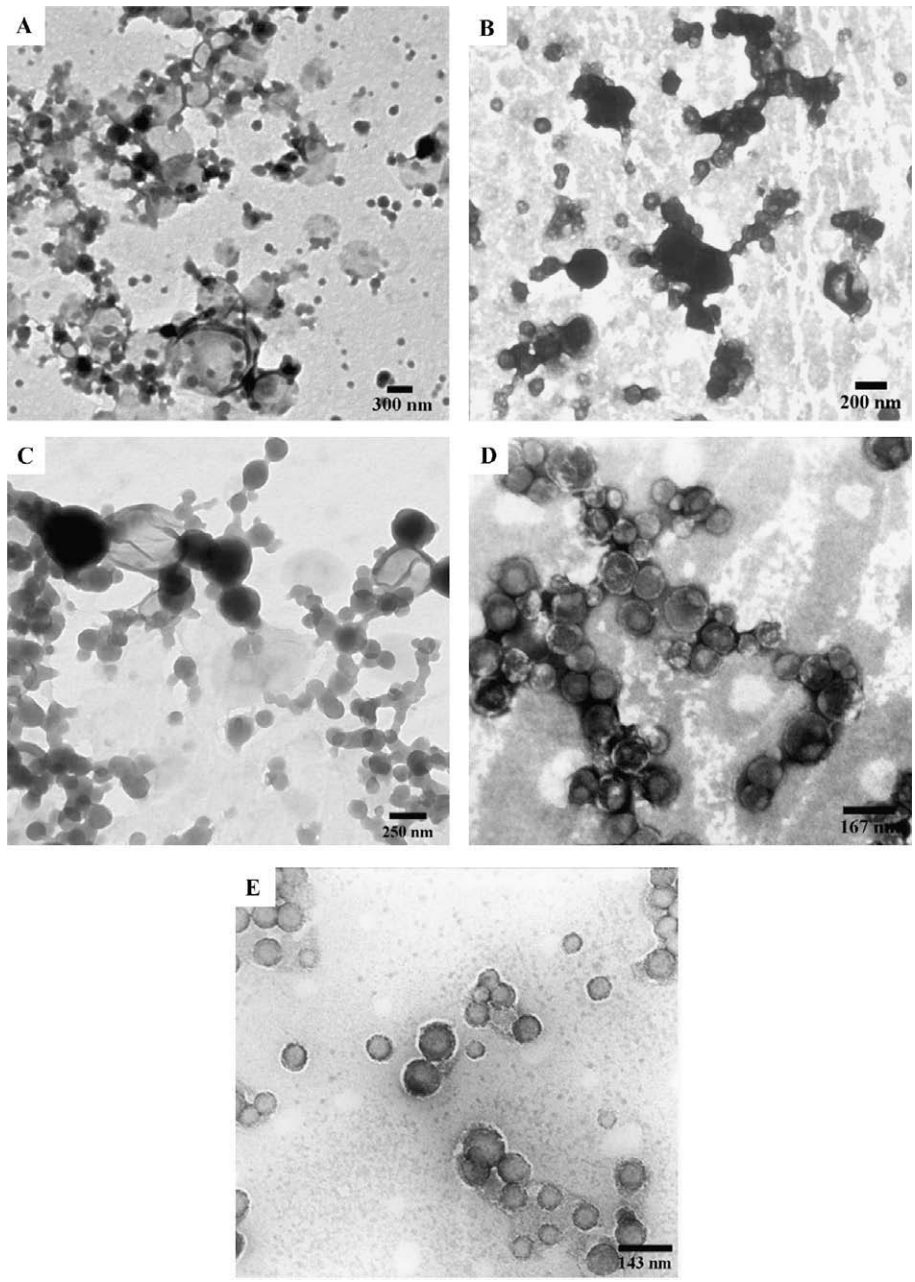

Fig. 4. TEM images of SVPh9-1/MVP8-2 hydrogen-bonded complexes in THF solution. (A) SVPh9-1/MVP8-2 = 1/1 and was stained with I_2 (B) SVPh9-1/MVP8-2 = 1/1 and was stained with RuO_4 (C) SVPh9-1/MVP8-2 = 1/2 and was stained with I_2 (D) SVPh9-1/MVP8-2 = 1/2 and was stained with RuO_4 and (E) RuO_4 stained sample of SVPh9-1/MVP8-2 = 1/0.5.

and swollen structures. As a result, the packing parameter will increase and the formation vesicles will be favored. Therefore, the vesicular complexes that formed in THF solution were surrounded by PMMA and PS chains. These micellar complexes are predicted to be very stable presumably because the PMMA and PS chains are soluble in THF; and enhance their stabilities in THF solution, therefore, these micelles do not precipitant in THF, which is contrast with the PVPh/P4VP homopolymer blend complexes [47,48].

Due to the strong hydrogen bonding between PVPh and P4VP blocks, the bound block possess extended conformation, which allows the bound copolymers chains to pack in parallel to form micelles with lamellae structures. At last it turns to vesicles in solution for minimizing surface energy. Therefore, the vesicular complexes are formed and surrounded by PMMA and PS chains in THF solution. These micellar complexes can be predicted to be very stable since these soluble PMMA and PS chains enhance the vesicular complex stabilities in THF solution. We believe that the in-

ner and outer layer polymer chains of vesicle are formed by PMMA and PS majority, respectively, because dark spots (PS staining with RuO_4) are outside aggregates as shown in Fig. 4B. Besides, PS and PMMA segments are mutually incompatible and immiscible and the PMMA also have the intermolecular hydrogen bonding with the PVPh based on FTIR analysis in Fig. 2(B). Therefore, the resulted vesicular complex is composed of an outer layer of PS block majority, a PVPh/P4VP complex aggregated wall, and an inner layer of PMMA block majority. The formation of the micellar complexes through hydrogen-bonding interaction between PVPh and P4VP in THF is schematically shown in Scheme 1 closed that shown in previous study [61].

Fig. 5 displays two differently sized vesicular micelles obtained at a PS-*b*-PVPh/PMMA-*b*-P4VP ratio of 1:4 ($M_{SH90\text{-}10}/M_{MVP80\text{-}20}$). Because RuO_4 was used to stain the sample, the visible part of the micelles must consist of PS, PVPh and P4VP blocks. Fig. 5(A) shows that some dark spots are present inside the larger vesicular micelles, but not fully in the hole; nevertheless, the dark spots of these larger vesicles are different from those observed in Fig. 4. We speculate that small aggregates and bilayers were formed during the early stages of micellization at a higher P4VP block content; these small aggregates were then underwent a wrapping process to form curved bilayers. As a result, the larger vesicular micelles contained some small aggregates, which appear as dark spots inside the vesicular micelles in Fig. 5(A). The enlarged image of the smaller-sized vesicles in Fig. 5(B) indicates that they possessed structures similar to those of regular vesicles.

Fig. 6 shows TEM images of mixtures of two block copolymers of longer complexation lengths (SVPh20-80/MVP35-65) at various molar ratios; the samples were stained with RuO_4 vapor. These micellar morphologies of SVPh20-80/MVP35-65 at 1/2, 1/1, and 1/0.5 molar ratios all exhibited vesicular structures [Fig. 6(A)–(C), respectively]. Thus, the inter-polymer hydrogen-bonded complexation between PS-*b*-PVPh and PMMA-*b*-P4VP in THF solution resulted in vesicular structures, regardless of the copolymer compositions, or and the molar ratio. The complexation between PVPh and P4VP blocks in THF favored to formation of vesicles in order to decrease the interfacial energy.

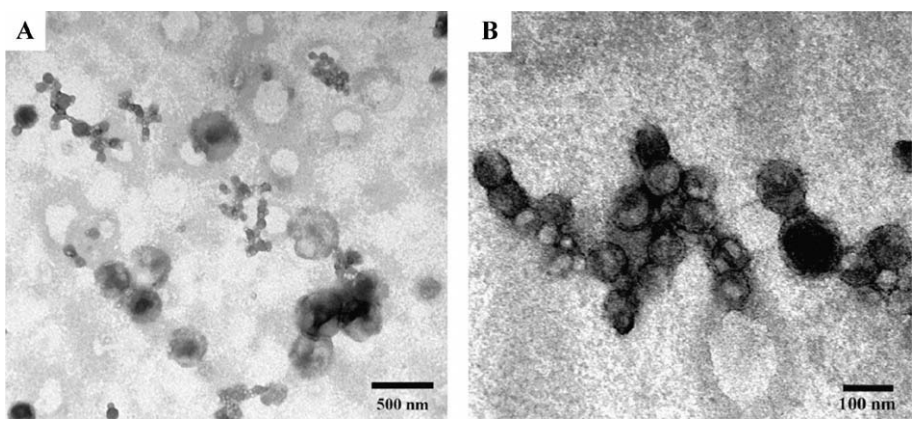

Fig. 5. (A) TEM images of RuO_4-stained samples obtained from a THF solution of SVPh90-10/ MVP80-20 (1/4). (B) Enlarged view of the small vesicular micelles in the sample in (A).

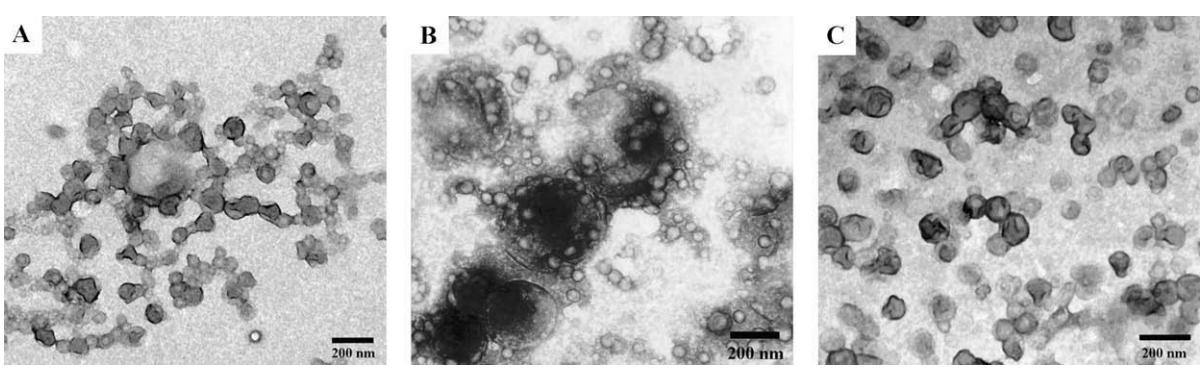

Fig. 6. TEM images of RuO_4-stained micelles formed in THF through inter-polymer hydrogen bond-mediated complexation of SVPh20-80/MVP35-65 at molar ratios of (A) 1/2, (B) 1/1, and (C) 1/0.5.

3.3. Structures and properties of PS-b-PVPH/PMMA-b-P4VP micelles in DMF solution

As we mentioned above, the hydrogen bonding between PS-*b*-PVPh and PMMA-*b*-P4VP in DMF is relatively weaker than that in THF solution as demonstrated by FTIR in Fig. 1. As a result, we expected to exhibit different morphologies compared with THF solution because of the higher mobility and swelling of the cores comprising the PVPh and P4VP blocks in DMF solution.

Initially, we used dynamic light scattering (DLS) to characterize the structures formed from the diblock copolymer mixtures in DMF. We analyzed the experimental correlation function using the cumulant method and the CONTIN algorithm, as described previously [50]. The Stokes–Einstein approximation was used to convert the diffusion coefficient into the form of the hydrodynamic diameter (D_h). Fig. 7 reveals that dependence of the hydrogen-bonding interaction on the PS_{90}-*b*-$PVPh_{10}$/$PMMA_{80}$-*b*-$P4VP_{20}$ ($M_{SH90\text{-}10}/M_{MVP80\text{-}20}$) ratio was complicated at a given polymer concentration. At an $M_{SH90\text{-}10}/M_{MVP80\text{-}20}$ molar ratio of 1/1, the largest peak associated with polymer aggregates appeared at a broad signal ca. 170 nm, providing direct evidence for hydrogen-bond mediated aggregate formation in PS_{90}-*b*-$PVPh_{10}$/$PMMA_{80}$-*b*-$P4VP_{20}$. At an $M_{SH90\text{-}10}/M_{MVP80\text{-}20}$ ratio of 1/2, the CONTIN size-distribution graph of this solution displayed a distribution equally as broad as that observed at 1/1 molar ratio. For the $M_{SH90\text{-}10}/M_{MVP80}$ = 1/0.5 mixtures, we observed micelles having a value of D_h of 100 nm. In addition, when the ratio of $M_{SH90\text{-}10}/M_{MVP80\text{-}20}$ = 1/1, 1/2, and 1/0.5, the DLS data contained small peaks located within the ranges from 6 to 12 nm, indicating that individual polymer chains were present. When the ratio was 1/0.5, the intensity of the small peak was highest, implying that more free polymer chains are existed as a result of an excess of donor group from the PS_{90}-*b*-$PVPh_{10}$ diblock polymer in the mixture. When the ratio was 1/4, only a monomodal distribution of micelles appeared, i.e., the small peak did not exist, suggesting that nearly all of the copolymer chains participated in the micelle blend. In addition, when the ratio was ca. 1:4, the value of D_h was minimized, implying that hydrogen bonding between PVPh and P4VP blocks was optimal at a lower PVPh content.

Fig. 8 illustrates several TEM images of the structures formed from SVPh90-10/MVP20-80 mixtures with various molar ratios in DMF. At a molar ratio of 1/4, we observed star-like micelles [Fig. 8(A)]; the presence of a dark core surrounded by a halo shell was confirmed by the optical density profile of the materials stained by I_2 at large magnification in Fig. 8(A). These cores, which formed through the hydrogen-bonding interactions between PVPh and P4VP blocks, were surrounded by coronas of soluble PMMA and PS chains. Because this copolymer mixture in DMF possesses relatively weaker hydrogen bonds in the core and higher solubility of its corona chains, the PVPh/P4VP blocks in the core have higher mobility and higher repulsion exists among the coronal chains (PS and PMMA blocks). Together, these phenomena induce the formation of spherical micelles, but with a mixed corona resulting from the presence of two different types of coronal blocks. In general, four types of mixed coronal spheres can exist [62]: (a) Janus (two-faced) spheres [63], (b) patched spheres [64–66], (c) uniformed spheres [67,68], (d) micelles having mixed coronas (no chain segregation) [30]. In our mixed diblock copolymer system, the coronal chains of PS and PMMA blocks were immiscible, and, therefore, they must likely formed spheres with chain-segregated coronas. Although, we could not detect such chain-segregated coronas when staining with I_2 because of poor selectivity between the PS and PMMA chains, we could contrast the micelles through RuO_4 staining to highlight the phase selectivity of their PS, PVPh, and P4VP blocks [Fig. 8(B)]. Small black spheres, resulting from different molecular

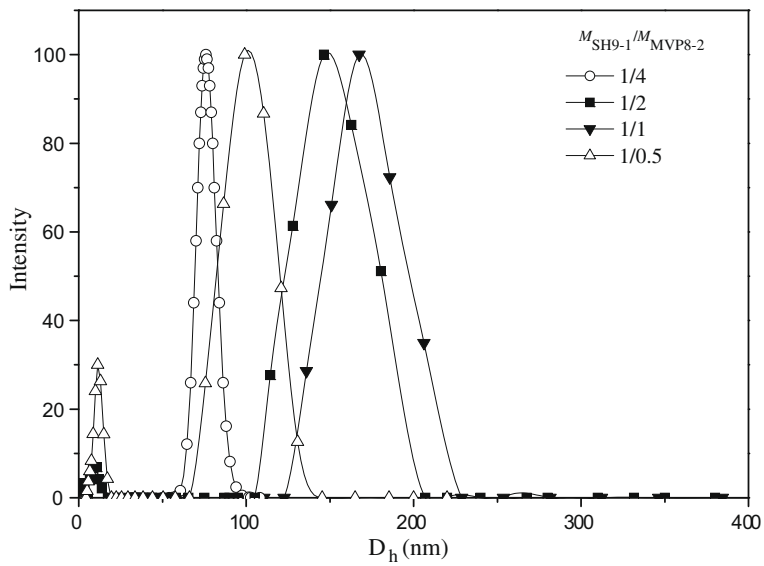

Fig. 7. Hydrodynamic diameters distributions of the SVPh90-10/MVP80-20 blend micelles formed at various molar ratios in DMF.

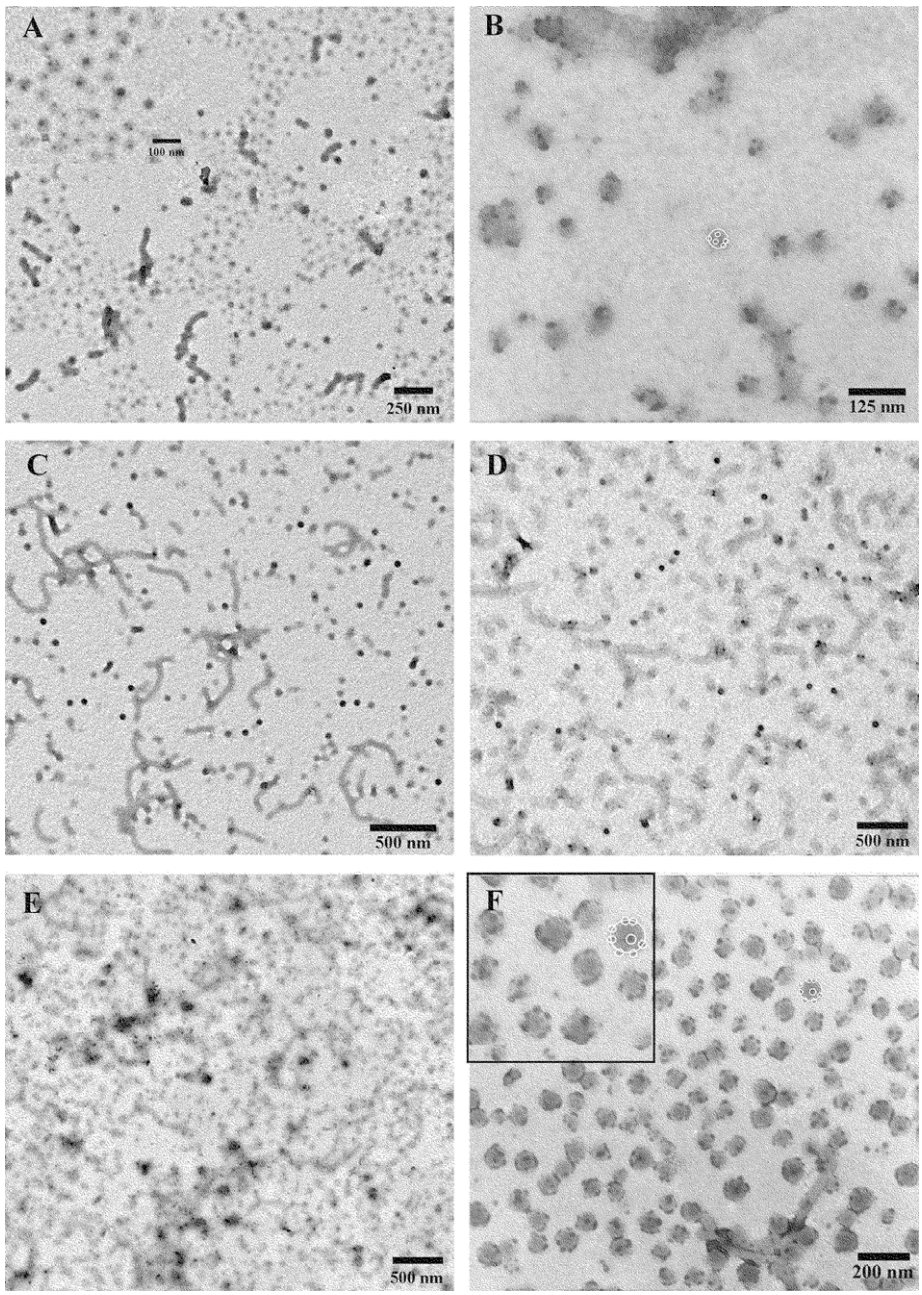

Fig. 8. TEM images of micelles formed in DMF from PS_{20}-*b*-$PVPh_{80}$/$PMMA_{35}$-*b*-$P4VP_{65}$ blends at molar ratios of (A) 1/4 (stained with I_2), (B) 1/4 (RuO_4), (C) 1/2 (I_2), (D) 1/2 (RuO_4), (E) 1/1 (I_2), and (F) 1/0.5 (RuO_4; the sample in the inset was stained with I_2).

weights of the PMMA and PS chains and their immiscibility, are clearly observed on the surfaces of the spherical micelles, indicating that the spheres must be of patched form; the image in the Scheme 1 present a schematic illustration of the micelles' structures. The diameter of these micelles, as measured from the TEM images, were within the range 50–55 nm, which are smaller values than those measured from DLS data; this situation arose because the samples for TEM observation were prepared through evaporation of the micelle particles and thus, chain collapse and micelle shrinkage was unavoidable. Although PS and PMMA chains are highly immiscible, we did not observe a Janus sphere in this case because DMF is a good solvent for both PS and PMMA chains. Two immiscible binary polymer blends can become miscible through the addition of a large amount of a good solvent, even though the PS and PMMA chains remain intrinsically immiscible. As a result, the patched sphere structure is a compromise phenomenon between these two phenomena.

By increasing the SVPh90-10/MVP80-20 content to molar ratios of 1/1 and 1/2, more rod-like micelles were formed [Fig. 8(C) and (E)]. The different morphologies that

formed upon varying the PS_{90}-*b*-$PVPh_{10}$ contents can be attributed to the increased number of donor groups of the PVPh blocks in the mixture. The original spherical micelles were surrounding by long PMMA chains, which can also act as proton acceptors, including hydrogen bonds between the PVPh and PMMA units, as indicated in Fig. 2(B). As a result, the rod-like micelles formed through intermolecular association between the PMMA corona and the PVPh core, with extended PMMA chains tending to penetrate into other spherical cores. We suspect that such phenomena explain why the spherical and rod-like micelles coexisted at higher PS-*b*-PVPh content in DMF system. When the samples were stained with RuO_4, the diameters of the spherical and rod-like micelles appeared to be slightly larger than those observed after I_2 staining [Fig. 8(D)] because the PS and PVPh blocks could be visualized also in the core–shell structures of the micellar aggregates. Because both spherical and a large number of rod-like micelles coexisted, the DLS measurements detect a broader distribution of micelles with a larger hydrodynamic diameter. At a copolymer mixture ratio = 1/0.5, fewer rod-like micelles were present (Fig. 8(F)) because of an excess of proton donors PS_{90}-*b*-$PVPh_{10}$ (or a lower content of proton acceptors $PMMA_{80}$-*b*-$P4VP_{20}$ content), fewer PMMA chains penetrating into other spherical cores, and some PMMA chains tending to shrink around the core by itself. Therefore, the majority of the bumpy spherical micelles observed at a molar ratio of 1/0.5 have a higher mean diameter than those at the 1/4 ratio. Fig. 8(F) shows a TEM image with high contrast for each spherical micelle, indicating that the longer PS blocks collapsed onto these surfaces so that the two phases (core and corona) could be distinguished clearly.

When the mixtures of the two block copolymers contained longer proton donor and acceptor lengths (SVPh20-80/MVP35-65) at various molar ratios, all of the micellar structures were spherical at 1/2, and 1/1 molar ratios [Fig. 9(A) and (B), respectively]. No rod-like micelles existed in the SVPh20-80/MVP35-65 systems at any composition because this system possesses much shorter coronal PMMA chains than did the SVPh90-10/MVP80-20 system. Shorter coronal PMMA chains have relatively fewer intermolecular interactions with the PVPh core and are unable to penetrate into other spherical cores. The spheres also appeared to be of patched form, but with larger cores than those obtained in the shorter inter-polymer hydrogen-bonding system. Fig. 8(C) presents the corresponding DLS results at molar ratios of 1/2, 1/1, and 1/0.5. Additional small peaks appeared in the ranges from 6 to 12 nm all molar ratios, indicating that the individual free polymer chains existed and that the broad mean-diameter distribution was due to the spheres having short coronal chains.

The main reason for the various morphologies of these diblock mixtures in THF and DMF solutions is the differing chain behavior of the PVPh and P4VP blocks. In THF, hydrogen bonds are maximized and the chain interaction could be highly stretched, thus favoring vesicles. In DMF, the complex are tightly bound and certainly characterized by a coil conformation that could explain the spherical morphology. The different chain length in these diblock copolymers mixture does not influence the self-assembly structure behavior in THF and DMF solutions, which is different with the bulk phase behavior of diblock copolymers mixture [9–11].

4. Conclusions

We have examined the coaggregation of PS-*b*-PVPh and PMMA-*b*-P4VP copolymers, with blocks of hydrogen bonding units of various lengths, in THF and DMF. Comicellization occurred through strong hydrogen bonding between the PVPh and P4VP blocks, leading to structures exhibiting different morphologies in THF and DMF solutions because DMF interfered with the hydrogen-bonding interactions between PVPh and P4VP to a greater extent than did THF. The inter-polymer hydrogen bonded-mediated complexation between PS-*b*-PVPh and PMMA-*b*-P4VP in THF resulted in lower-mobility of PVPh/P4VP complex cores and vesicular complexes surrounded by PMMA and PS chains. In contrast, the systems in DMF possessed highly swollen PVPh/P4VP blend cores and a patched distribution of PS and PMMA as coronas. Scheme 1 illustrates the formation of these vesicular and patched spherical micellar complexes and the possible mechanism of micellization medi-

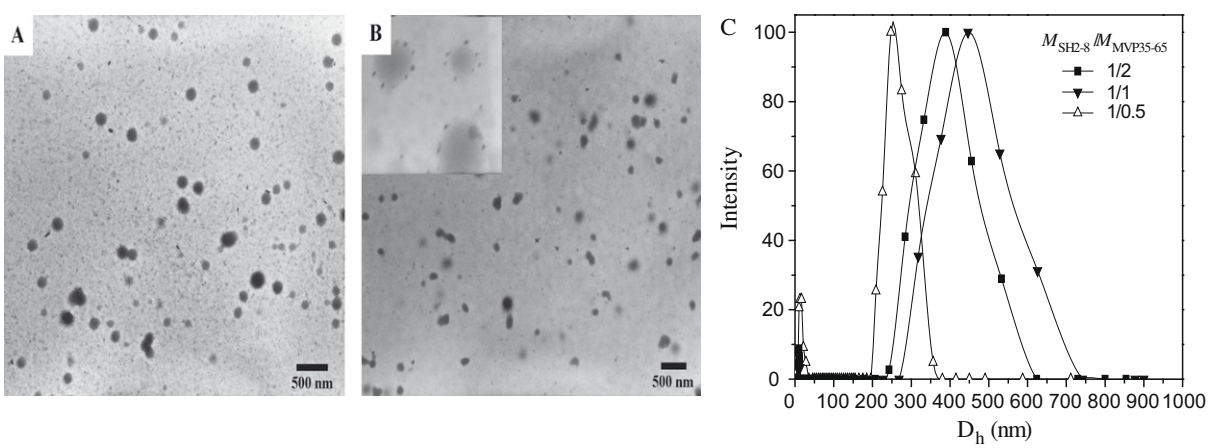

Fig. 9. TEM images of micelles formed in DMF from PS_{20}-*b*-$PVPh_{80}$ /$PMMA_{35}$-*b*-$P4VP_{65}$ blends at molar ratios of (A) 1/2 (stained with I_2), and (B) 1/1 (I_2; the sample in the inset was stained with RuO_4. (C) CONTIN size-distribution of the micelles as measured using DLS.

ated by hydrogen-bonding interactions between complementary polymers.

Acknowledgments

This work was supported financially by the National Science Council, Taiwan, Republic of China, under Contract Nos. NSC 97-2221-E-110-013-MY3 and NSC 97-2120-M-009-003.

References

[1] Patten TE, Matyjaszewski K. Adv Mater 1998;10:901.
[2] Sakurai S, Kawada H, Hashimoto T, Fetter LJ. Macromolecules 1993;26:5796.
[3] Hamley IW. The physicals of block copolymers. New York: Oxford University Press; 1998.
[4] Kreutzer G, Ternat C, Nguyen TQ, Plummer CJG, Manson JAE, Castelletto V, et al. Macromolecules 2006;39:4507.
[5] Cong Y, Li B, Han Y, Li Y, Pan C. Macromolecules 2005;38:9836.
[6] Chan SC, Kuo SW, Lu CH, Lee HF, Chang FC. Polymer 2007;48:5059.
[7] Hadjichristidis N, Iatrou H, Pitsikalis M, Pispas S, Avgeropoulous A. Prog Polym Sci 2005;30:725.
[8] Tung PH, Kuo SW, Chang FC. Polymer 2007;48:3192.
[9] Asari T, Matsuo S, Takano A, Matsushita Y. Macromolecules 2005;38:8811.
[10] Asari T, Matsuo S, Takano A, Matsushita Y. Macromolecules 2006;39:2232.
[11] Matsushita Y. Macromolecules 2007;40:771.
[12] Zheng R, Liu G, Yan X. J Am Chem Soc 2005;127:15358.
[13] Zhang L, Eisenberg A. Polym Adv Technol 1998;9:677.
[14] Riess GA. Prog Polym Sci 2003;28:1107.
[15] Rodriguez-Hernandez J, Checot F, Gnanou Y, Lecommandoux S. Prog Polym Sci 2005;30:691.
[16] Kataoka K, Kwon GS, Yokoyama Y, Okano T, Sakurai Y. J Control Release 1993;24:119.
[17] Kitazawa Y, Miyata F, Kataoka SK. Adv Mater 2004;16:699.
[18] Yan X, Liu G, Haeussler M, Tang BZ. Chem Mater 2005;17:6053.
[19] Aizawa M, Buriak JM. J Am Chem Soc 2005;127:8932.
[20] Djalali R, Li SY, Schmidt M. Macromolecules 2002;35:4282.
[21] Selvan ST, Hayakawa T, Nogami M, Moller M. J Phys Chem B 1999;103:7441.
[22] Wang XS, Wang H, Coombs N, Winnik MA, Manners I. J Am Chem Soc 2005;127:8924.
[23] Kabanov AV, Bronich TK, Kabanov VA, Yu K, Eisenberg A. Macromolecules 1996;29:6797.
[24] Bronich TK, Kabanov AV, Kabanov VA, Yu K, Eisenberg A. Macromolecules 1997;30:3519.
[25] Lysenko EA, Bronich TK, Eisenberg A, Kabanov VA, Kabanov AV. Macromolecules 1998;31:4516.
[26] Bronich TK, Popov AM, Eisenberg A, Kabanov VA, Kabanov AV. Langmuir 2000;16:481.
[27] Lefevre N, Fustin LA, Varshney SK, Gohy JF. Polymer 2007;48:2306.
[28] Gohy JF, Khousakoun E, Willet N, Varshney SK, Jerome R. Macromol Rapid Commun 2004;25:1536.
[29] Hu J, Liu G. Macromolecules 2005;38:8058.
[30] Yan XH, Liu G. Macromolecules 2006;39:1906.
[31] Lee SC, Kim KJ, Jeong YK, Chang JH, Choi J. Macromolecules 2005;38:9291.
[32] Gao WP, Bai Y, Chen EQ, Li ZC, Han BY, Yang WT, et al. Macromolecules 2006;39:4894.
[33] Zhang W, Shi L, Gao L, An Y, Li G, Wu K, et al. Macromolecules 2005;38:899.
[34] Li G, Shi L, Ma R, An Y, Huang N. Angew Chem Int Ed 2006;45:4959.
[35] Kuo SW, Tung PH, Lai CL, Jeong KU, Chang FC. Macromol Rapid Commun 2008;29:229.
[36] Chen D, Jiang M. Acc Chem Res 2005;38:494.
[37] Yan X, Liu G, Hu J, Willson CG. Macromolecules 2006;39:1906.
[38] Gohy JF, Varshney SK, Jerome R. Macromolecules 2001;34:3361.
[39] Harada A, Kataoka K. Science 1999;283:65.
[40] Fukushima S, Miyata K, Nishiyama N, Kanayama N, Yamasaki Y, Kataoka K. J Am Chem Soc 2005;127:2810.
[41] Schrage S, Sigel R, Schlaad H. Macromolecules 2003;36:1417.
[42] Gohy JF, Hofmeier H, Alexeev A, Schubert US. Macromol Chem Phys 2003;204:1524.
[43] Zhang GZ, Liu S, Zhao H, Jiang M. Mater Sci Eng C 1999;10:155.
[44] Talingting MR, Munk P, Webber SE, Tuzar Z. Macromolecules 1999;32:1593.
[45] Li Z, Kesselman E, Talmon Y, Hillmyer M, Lodge T. Science 2004;306:98.
[46] Kubowicz S, Baussard JF, Lutz JF, Thünemann AF, Berlepsch H, Laschewsky A. Angew Chem Int Ed 2005;44:5262.
[47] Dai J, Goh SH, Lee SY, Siow KS. Polym J 1994;26:905.
[48] Wang LF, Pearce EM, Kwei TK. J Polym Sci Polym Phys Ed 1991;29:619.
[49] Coleman MM, Graf JF, Painter PC. In: Specific interactions and the miscibility of polymer blends. Lancaster, PA: Technomic Publishing; 1991.
[50] Lee HF, Kuo SW, Huang CF, Lu JS, Chan SC, Wang CF, et al. Macromolecule 2006;39:5458.
[51] Kuo SW, Chan SC, Chang FC. Macromolecules 2003;36:6653.
[52] Kuo SW, Liu WP, Chang FC. Macromolecules 2003;36:5165.
[53] Kuo SW, Chang FC. Macromolecules 2001;34:5224.
[54] Kuo SW, Tung PH, Chang FC. Macromolecules 2006;39:9388.
[55] Jiang M, Li M, Xiang M, Zhou H. Adv Polym Sci 1999;146:121.
[56] Ndoni S, Papadakis CM, Bates FS, Almdal K. Rev Sci Instrum 1995;66:1090.
[57] Li M, Douki K, Goto K, Li X, Coenjarts C, Smilgies DM, et al. Chem Mater 2004;16:3800.
[58] Lin CL, Chen WC, Liao CS, Su YC, Huang CF, Kuo SW, et al. Macromolecules 2005;38:6435.
[59] Tung PH, Kuo SW, Jeong KW, Cheng SZD, Huang CF, Chang FC. Macromol Rapid Commun 2007;207:271.
[60] Kuo SW, Lin CL, Chang FC. Polymer 2002;43:3943.
[61] Zheng R, Liu G. J Am Chem Soc 2005;124:15358.
[62] Hoppenbrouwers E, Li Z, Liu G. Macromolecules 2003;36:876.
[63] Erhardt R, Boker A, Zettl H, Kaya H, Pyckhout-Hintzen W, Krausch G, et al. Macromolecules 2001;34:1069.
[64] Hu Y, Zhang L, Cao Y, Ge H, Jiang X, Yang C. Biomacromolecules 2004;5:1756.
[65] Gohy JF, Varshney SK, Antoun S, Jerome R. Macromolecules 2000;33:9298.
[66] Battaglia G, Ryan AJ. J Am Chem Soc 2005;127:8757.
[67] Xie D, Xu K, Bai R, Zhang G. J Phys Chem B 2007;111:778.
[68] Fustin CA, Abetz V, Gohy JF. Eur Phys J E 2005;16:291.